Plasmonic coaxial waveguide-cavity devices

Amirreza Mahigir,[1,2] **Pouya Dastmalchi,**[1,2] **Wonseok Shin,**[3] **Shanhui Fan,**[3] **and Georgios Veronis**[1,2,*]

[1] *School of Electrical Engineering and Computer Science, Louisiana State University, Baton Rouge, Louisiana 70803, USA*
[2] *Center for Computation and Technology, Louisiana State University, Baton Rouge, Louisiana 70803, USA*
[3] *E. L. Ginzton Laboratory, Stanford University, Stanford, California 94305, USA*
[*] *gveronis@lsu.edu*

Abstract: We theoretically investigate three-dimensional plasmonic waveguide-cavity structures, built by side-coupling stub resonators that consist of plasmonic coaxial waveguides of finite length, to a plasmonic coaxial waveguide. The resonators are terminated either in a short or an open circuit. We show that the properties of these waveguide-cavity systems can be accurately described using a single-mode scattering matrix theory. We also show that, with proper choice of their design parameters, three-dimensional plasmonic coaxial waveguide-cavity devices and two-dimensional metal-dielectric-metal devices can have nearly identical transmission spectra. Thus, three-dimensional plasmonic coaxial waveguides offer a platform for practical implementation of two-dimensional metal-dielectric-metal device designs.

OCIS codes: (240.6680) Surface plasmons; (260.3910) Metal optics; (130.2790) Guided waves.

References and links

1. W. L. Barnes, A. Dereux, and T. W. Ebbesen, "Surface plasmon subwavelength optics," Nature (London) **424**, 824–830 (2003).
2. E. Ozbay, "Plasmonics: merging photonics and electronics at nanoscale dimensions," Science **311**, 189–193 (2006).
3. R. Zia, J. A. Schuller, A. Chandran, and M. L. Brongersma, "Plasmonics: the next chip-scale technology," Mater. Today **9**, 20–27 (2006).
4. S. A. Maier and H. A. Atwater, "Plasmonics: Localization and guiding of electromagnetic energy in metal/dielectric structures," J. Appl. Phys. **98**, 011101 (2005).
5. J. A. Schuller, E. S. Barnard, W. Cai, Y. C. Jun, J. S. White, and M. L. Brongersma, "Plasmonics for extreme light concentration and manipulation," Nat. Mater. **9**, 193–204 (2010).
6. D. K. Gramotnev and S. I. Bozhevolnyi, "Plasmonics beyond the diffraction limit," Nat. Photonics **4**, 83–91 (2010).
7. Z. Han and S. I. Bozhevolnyi, "Radiation guiding with surface plasmon polaritons," Rep. Prog. Phys. **76**, 016402 (2013).
8. J. A. Dionne, L. A. Sweatlock, M. T. Sheldon, A. P. Alivisatos, and H. A. Atwater, "Silicon-based plasmonic for on-chip photonics," IEEE J. Sel. Top. Quantum Electron. **16**, 295–306 (2010).
9. J. Takahara, S. Yamagishi, H. Taki, A. Morimoto, and T. Kobayashi, "Guiding of a one-dimensional optical beam with nanometer diameter," Opt. Lett. **22**, 475–477 (1997).
10. Y. Bian and Q. Gong, "Tuning the hybridization of plasmonic and coupled dielectric nanowire modes for high-performance optical waveguiding at sub-diffraction-limited scale," Sci. Rep. **4**, 6617 (2014).
11. Y. Bian and Q. Gong, "Deep-subwavelength light routing in nanowire-loaded surface plasmon polariton waveguides: an alternative to the hybrid guiding scheme," J. Phys. D: Appl. Phys. **46**, 445105 (2013).

#242538 Received 8 Jun 2015; revised 16 Jul 2015; accepted 23 Jul 2015; published 28 Jul 2015

12. S. I. Bozhevolnyi, V. S. Volkov, E. Devaux, J.-Y. Laluet, and T. W. Ebbesen, “Channel plasmon subwavelength waveguide components including interferometers and ring resonators,” Nature (London) **440**, 508–511 (2006).
13. D. F. Pile and D. K. Gramotnev, “Plasmonic subwavelength waveguides: next to zero losses at sharp bends,” Opt. Lett. **30**, 1186–1188 (2005).
14. Y. Zhu, X. Hu, H. Yang, and Q. Gong, “On-chip plasmon-induced transparency based on plasmonic coupled nanocavities,” Sci. Rep. **4**, 3752 (2014).
15. S. Zhu, G. Lo, and D. Kwong, “Nanoplasmonic power splitters based on the horizontal nanoplasmonic slot waveguide,” Appl. Phys. Lett. **99**, 031112 (2011).
16. Y. Bian and Q. Gong, “Metallic-nanowire-loaded silicon-on-insulator structures: a route to low-loss plasmon waveguiding on the nanoscale,” Nanoscale **7**, 4415–4422 (2015).
17. R. F. Oulton, V. J. Sorger, D. A. Genov, D. F. P. Pile, and X. Zhang, “A hybrid plasmonic waveguide for subwavelength confinement and long-range propagation,” Nat. Photonics **2**, 496–500 (2008).
18. Y. Bian and Q. Gong, “Deep-subwavelength light confinement and transport in hybrid dielectric-loaded metal wedges,” Laser Photon. Rev. **8**, 549–561 (2014).
19. G. Veronis and S. Fan, “Modes of subwavelength plasmonic slot waveguides,” J. Lightwave Technol. **25**, 2511–2521 (2007).
20. W. Cai, W. Shin, S. Fan, and M. L. Brongersma, “Elements for plasmonic nanocircuits with three-dimensional slot waveguides,” Adv. Mater. **22**, 5120–5124 (2010).
21. J. A. Dionne, H. J. Lezec, and H. A. Atwater, “Highly confined photon transport in subwavelength metallic slot waveguides,” Nano Lett. **6**, 1928–1932 (2006).
22. Y. Fu, X. Hu, C. Lu, S. Yue, H. Yang, and Q. Gong, “All-optical logic gates based on nanoscale plasmonic slot waveguides,” Nano Lett. **12**, 5784–5790 (2012).
23. S. A. Maier, *Plasmonics: Fundamentals and Applications* (Springer, 2007).
24. R. Zia, M. D. Selker, P. B. Catrysse, and M. L. Brongersma, “Geometries and materials for subwavelength surface plasmon modes,” J. Opt. Soc. Am. A **21**, 2442–2446 (2004).
25. J. A. Dionne, L. A. Sweatlock, H. A. Atwater, and A. Polman, “Planar metal plasmon waveguides: frequency-dependent dispersion, propagation, localization, and loss beyond the free electron model,” Phys. Rev. B **72**, 075405 (2005).
26. H. Shin, M. F. Yanik, S. Fan, R. Zia, and M. L. Brongersma, “Omnidirectional resonance in a metal–dielectric–metal geometry,” Appl. Phys. Lett. **84**, 4421–4423 (2004).
27. E. Verhagen, J. A. Dionne, L. Kuipers, H. A. Atwater, and A. Polman, “Near-field visualization of strongly confined surface plasmon polaritons in metal- insulator- metal waveguides,” Nano Lett. **8**, 2925–2929 (2008).
28. H. J. Lezec, J. A. Dionne, and H. A. Atwater, “Negative refraction at visible frequencies,” Science **316**, 430–432 (2007).
29. P. Neutens, P. Van Dorpe, I. De Vlaminck, L. Lagae, and G. Borghs, “Electrical detection of confined gap plasmons in metal–insulator–metal waveguides,” Nat. Photonics **3**, 283–286 (2009).
30. C.-I. Lin and T. K. Gaylord, “Multimode metal-insulator-metal waveguides: Analysis and experimental characterization,” Phys. Rev. B **85**, 085405 (2012).
31. G. Veronis and S. Fan, “Bends and splitters in subwavelength metal-dielectric-metal plasmonic waveguides,” Appl. Phys. Lett. **87**, 131102 (2005).
32. W. Shin, W. Cai, P. B. Catrysse, G. Veronis, M. L. Brongersma, and S. Fan, “Broadband sharp 90-degree bends and T-splitters in plasmonic coaxial waveguides,” Nano Lett. **13**, 4753–4758 (2013).
33. X.-S. Lin and X.-G. Huang, “Tooth-shaped plasmonic waveguide filters with nanometeric sizes,” Opt. Lett. **33**, 2874–2876 (2008).
34. Y. Huang, C. Min, L. Yang, and G. Veronis, “Nanoscale plasmonic devices based on metal-dielectric-metal stub resonators,” Int. J. Opt. **2012**, 372048 (2012).
35. A. Hosseini and Y. Massoud, “Nanoscale surface plasmon based resonator using rectangular geometry,” Appl. Phys. Lett. **90**, 181102 (2007).
36. I. Zand, A. Mahigir, T. Pakizeh, and M. S. Abrishamian, “Selective-mode optical nanofilters based on plasmonic complementary split-ring resonators,” Opt. Express **20**, 7516–7525 (2012).
37. C. Min and G. Veronis, “Absorption switches in metal-dielectric-metal plasmonic waveguides,” Opt. Express **17**, 10757–10766 (2009).
38. L. Yang, C. Min, and G. Veronis, “Guided subwavelength slow-light mode supported by a plasmonic waveguide system,” Opt. Lett. **35**, 4184–4186 (2010).
39. Y. Huang, C. Min, and G. Veronis, “Subwavelength slow-light waveguides based on a plasmonic analogue of electromagnetically induced transparency,” Appl. Phys. Lett. **99**, 143117 (2011).
40. A. Pannipitiya, I. D. Rukhlenko, M. Premaratne, H. T. Hattori, and G. P. Agrawal, “Improved transmission model for metal-dielectric-metal plasmonic waveguides with stub structure,” Opt. Express **18**, 6191–6204 (2010).
41. Z.-J. Zhong, Y. Xu, S. Lan, Q.-F. Dai, and L.-J. Wu, “Sharp and asymmetric transmission response in metal-dielectric-metal plasmonic waveguides containing Kerr nonlinear media,” Opt. Express **18**, 79–86 (2010).
42. J. Liu, G. Fang, H. Zhao, Y. Zhang, and S. Liu, “Surface plasmon reflector based on serial stub structure,” Opt. Express **17**, 20134–20139 (2009).

#242538 Received 8 Jun 2015; revised 16 Jul 2015; accepted 23 Jul 2015; published 28 Jul 2015

43. F. Hu, H. Yi, and Z. Zhou, "Wavelength demultiplexing structure based on arrayed plasmonic slot cavities," Opt. Lett. **36**, 1500–1502 (2011).
44. S. R. Mirnaziry, A. Setayesh, and M. S. Abrishamian, "Design and analysis of plasmonic filters based on stubs," J. Opt. Soc. Am. B **28**, 1300–1307 (2011).
45. G. Veronis and S. Fan, "Overview of simulation techniques for plasmonic devices," in *Surface Plasmon Nanophotonics*, M. L. Brongersma and P. G. Kik, eds. (Springer, 2007), pp. 169–182.
46. W. Shin and S. Fan, "Accelerated solution of the frequency-domain Maxwell's equations by engineering the eigenvalue distribution of the operator," Opt. Express **21**, 22578–22595 (2013).
47. E. D. Palik, *Handbook of Optical Constants of Solids*, Vol. 3 (Academic, 1985).
48. J. Jin, *The Finite Element Method in Electromagnetics* (John Wiley & Sons, 2014).
49. W. Shin and S. Fan, "Choice of the perfectly matched layer boundary condition for frequency-domain Maxwell's equations solvers," J. Comput. Phys. **231**, 3406–3431 (2012).
50. S. E. Kocabas, G. Veronis, D. A. B. Miller, and S. Fan, "Transmission line and equivalent circuit models for plasmonic waveguide components," IEEE J. Sel. Top. Quantum Electron. **14**, 1462–1472 (2008).
51. J.-S. Huang, T. Feichtner, P. Biagioni, and B. Hecht, "Impedance matching and emission properties of nanoantennas in an optical nanocircuit," Nano Lett. **9**, 1897–1902 (2009).
52. D. M. Pozar, *Microwave Engineering* (John Wiley & Sons, 2009).
53. D. Pacifici, H. J. Lezec, H. A. Atwater, and J. Weiner, "Quantitative determination of optical transmission through subwavelength slit arrays in Ag films: Role of surface wave interference and local coupling between adjacent slits," Phys. Rev. B **77**, 115411 (2008).
54. D. Pacifici, H. J. Lezec, L. A. Sweatlock, R. J. Walters, and H. A. Atwater, "Universal optical transmission features in periodic and quasiperiodic hole arrays," Opt. Express **16**, 9222–9238 (2008).
55. G. Wang, H. Lu, and X. Liu, "Dispersionless slow light in MIM waveguide based on a plasmonic analogue of electromagnetically induced transparency," Opt. Express **20**, 20902–20907 (2012).
56. B. Yun, G. Hu, and Y. Cui, "Systematical research on the plasmon-induced transparency in coupled plasmonic resonators," Opt. Commun. **305**, 17–22 (2013).
57. G. Cao, H. Li, Y. Deng, S. Zhan, Z. He, and B. Li, "Plasmon-induced transparency in a single multimode stub resonator," Opt. Express **22**, 25215–25223 (2014).
58. B. Yun, G. Hu, C. Jiawei, and Y. Cui, "Plasmon induced transparency in metal–insulator–metal waveguide by a stub coupled with F-P resonator," Mater. Res. Express **1**, 036201 (2014).
59. P. Dastmalchi and G. Veronis, "Efficient design of nanoplasmonic waveguide devices using the space mapping algorithm," Opt. Express **21**, 32160–32175 (2013).
60. M. L. Povinelli, S. G. Johnson, S. Fan, and J. D. Joannopoulos, "Emulation of two-dimensional photonic crystal defect modes in a photonic crystal with a three-dimensional photonic band gap," Phys. Rev. B **64**, 075313 (2001).
61. G. Veronis and S. Fan, "Theoretical investigation of compact couplers between dielectric slab waveguides and two-dimensional metal-dielectric-metal plasmonic waveguides," Opt. Express **15**, 1211–1221 (2007).

---

1. Introduction

Plasmonic waveguides enable subwavelength confinement of optical modes, and are therefore important for achieving nanoscale integrated photonic devices [1–18]. In particular, plasmonic two-conductor waveguides support a subwavelength quasi-transverse-electromagnetic (quasi-TEM) propagating mode at a broad wavelength range which extends into the infrared and visible [19–22]. Two-dimensional (2D) metal-dielectric-metal (MDM) plasmonic waveguides, which are an example of such plasmonic two-conductor waveguides, have been investigated in detail both theoretically [23–26] and experimentally [21, 27–30]. For such waveguides it has been demonstrated that one can design sharp 90° bends and T-splitters with no additional loss on top of the material loss in the metal over a very wide frequency range [31]. Sharp 90° bends and T-splitters have also been recently demonstrated for three-dimensional (3D) plasmonic coaxial waveguides with square cross section, which can be fabricated using lithography-based techniques [32]. In addition, waveguide-cavity systems are particularly useful for the development of several integrated photonic devices, such as optical switches, sensors, filters, reflectors, and impedance matching elements. Several 2D plasmonic waveguide-cavity systems have been theoretically investigated [33–44].

In this paper, we theoretically investigate 3D plasmonic waveguide-cavity structures, built by side-coupling stub resonators that consist of plasmonic coaxial waveguides of finite length, to a plasmonic coaxial waveguide. We first investigate structures consisting of a single plasmonic coaxial resonator, which is terminated either in a short or an open circuit. We find that, in contrast to open-circuited 2D MDM plasmonic waveguides which suffer from large radiation losses, open-circuited plasmonic coaxial waveguides have very small radiation losses, and can therefore be used as resonators in waveguide-cavity devices. We show that the incident waveguide mode is almost completely reflected on resonance, while far from the resonance the waveguide mode is almost completely transmitted. We next consider waveguide-cavity structures built by side-coupling a plasmonic coaxial waveguide to two open-circuited stub resonators. We show that this structure is a plasmonic classical analogue of electromagnetically-induced transparency (EIT), and exhibits EIT-like transmission spectra, consisting of a transparency peak in the center of a broader transmission dip.

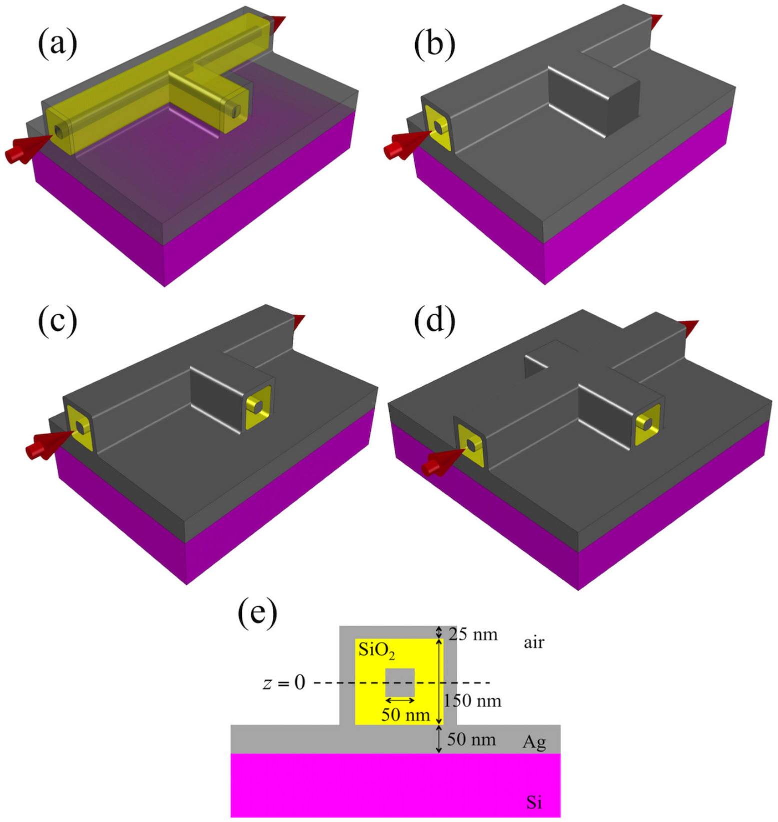

Fig. 1. (a) Schematic of a plasmonic coaxial waveguide side-coupled to a coaxial stub resonator. The propagation direction of light is indicated by red arrows. (b-d) Structures of a plasmonic coaxial waveguide side-coupled to a short-circuited, an open-circuited, and two open-circuited coaxial stub resonators. (e) Cross section of the reference plasmonic coaxial waveguide. Silver is used as the metal.

We also show that the properties of the waveguide-cavity systems can be accurately described using a single-mode scattering matrix theory. The transmission and reflection coefficients at waveguide junctions can be numerically extracted using full-wave simulations, and the results obtained with scattering matrix theory using this approach are in all cases in very good agreement with the exact results. These coefficients can also be predicted using transmission line theory and the concept of characteristic impedance. Despite its limited accuracy, the

#242538 Received 8 Jun 2015; revised 16 Jul 2015; accepted 23 Jul 2015; published 28 Jul 2015

transmission line model is computationally efficient, and, when combined with space mapping algorithms, it could enable the efficient design of nanoplasmonic coaxial waveguide devices. Finally we show that, with proper choice of their design parameters, a 3D plasmonic coaxial waveguide-cavity device and a 2D MDM device can have nearly identical transmission spectra. Thus, 3D plasmonic coaxial waveguides offer a platform for practical implementation of 2D MDM device designs.

The remainder of the paper is organized as follows. In Sections 2 and 3, we investigate structures consisting of a plasmonic coaxial waveguide side-coupled to a single coaxial resonator, which is terminated in a short circuit and open circuit, respectively. In Section 4, we investigate structures consisting of a plasmonic coaxial waveguide side-coupled to two open-circuited coaxial stub resonators. In Section 5, we discuss the emulation of 2D MDM plasmonic waveguide devices with 3D coaxial waveguide devices. Finally, our conclusions are summarized in Section 6.

2. Plasmonic coaxial waveguide side-coupled to a short-circuited coaxial stub resonator

Figure 1(a) shows a schematic of the waveguide-cavity structures investigated in this paper. They are built by side-coupling a stub resonator, consisting of a plasmonic coaxial waveguide of finite length, to a plasmonic coaxial waveguide. The metal used is silver, and the space between the metallic parts is filled with silica. The structures are placed on top of a silicon substrate. If the inner and outer metals at the end of the stub are connected [Fig. 1(b)], the stub is short-circuited. Otherwise, it is open-circuited [Fig. 1(c)].

Figure 2(a) shows the top view schematic at $z = 0$ of a plasmonic coaxial waveguide, coupled to a short-circuited stub resonator [Fig. 1(e)]. The power transmission characteristics of the device are investigated using the 3D finite-difference frequency-domain (FDFD) method [45, 46]. This method allows us to directly use experimental data for dispersive materials such as silver [47], including both the real and imaginary parts, with no approximation. We use the stretched-coordinate perfectly matched layer (SC-PML) absorbing boundary conditions at all boundaries of the simulation domain [48, 49]. To calculate the power transmission coefficient of the devices, their output power is normalized by the output power from a straight waveguide of the same length.

Figure 2(e) shows the power transmission coefficient of the coaxial waveguide side-coupled to the short-circuited coaxial stub resonator as a function of the stub length, obtained from full-wave FDFD simulations (dots). The operation wavelength is $\lambda_0 = 1550$ nm. At this wavelength the guide wavelength of the fundamental mode of the plasmonic coaxial waveguide was found to be $\lambda_g \simeq 680$ nm. We observe that the transmission becomes zero when the length of the stub is approximately equal to 290 nm. The metal at the end of the short-circuited stub and the inner metal of the main waveguide form a cavity resonator. The required stub length for zero transmission can be estimated based on the dimensions of this cavity. Since the cavity is short-circuited at both sides, its first resonance length will be $L_c = \lambda_g/2 \simeq 340$ nm, where L_c is the cavity length. The distance between the inner and outer metal of the plasmonic waveguide is $w = 50$ nm [Fig. 1(e)]. The required stub length can therefore be estimated as $L = L_c - w \simeq 290$ nm, which is in agreement with the numerically calculated value [Fig. 2(e)]. Similarly, the second resonance length can be estimated as $L_c = \lambda_g \simeq 680$ nm, and therefore the required stub length for the second resonance is $L = L_c - w \simeq 630$ nm. This is again in good agreement with the numerically calculated value which we found to be 625 nm.

Figures 2(f) and 2(g) show the profile of the H_z field component for two different lengths of the stub resonator. For $L = 290$ nm the cavity is on resonance. Since the directly transmitted wave destructively interferes with the decaying amplitude into the forward direction of the resonant cavity field, the transmission is approximately zero [Fig. 2(f)]. For $L = 460$ nm the

#242538 Received 8 Jun 2015; revised 16 Jul 2015; accepted 23 Jul 2015; published 28 Jul 2015

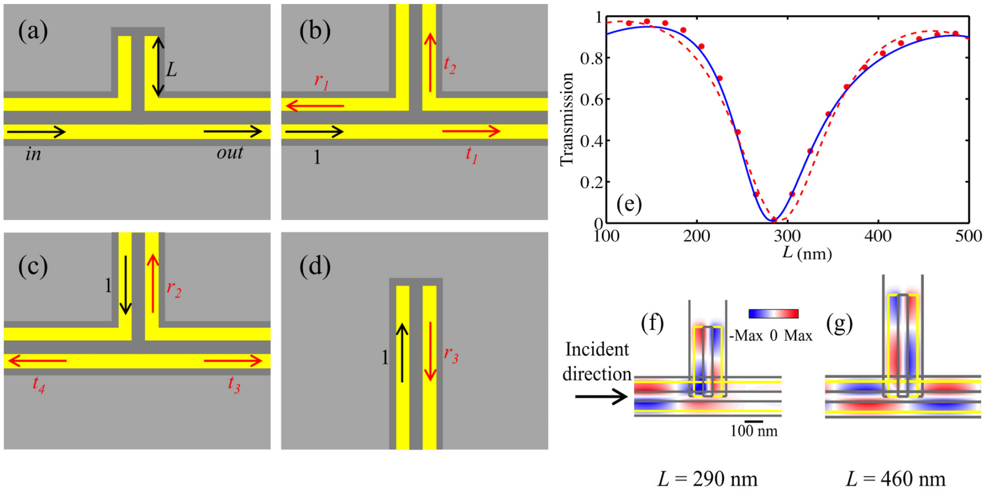

Fig. 2. (a) Top view schematic at $z = 0$ [Fig. 1(e)] of a plasmonic coaxial waveguide side-coupled to a short-circuited coaxial stub resonator. (b and c) Schematics defining the reflection coefficients r_1 and r_2, and transmission coefficients t_1, t_2, t_3, and t_4, when the fundamental mode of the plasmonic coaxial waveguide is incident at a T-splitter. Note that $t_3 = t_4$ due to symmetry. (d) Schematic defining the reflection coefficient r_3 of the fundamental mode of the plasmonic coaxial waveguide at the boundary of a short-circuited coaxial waveguide. (e) Transmission as a function of the stub length L for the structure of (a), calculated using FDFD (dots), scattering matrix theory with numerically calculated coefficients (blue solid line), and scattering matrix theory with coefficients calculated based on transmission line model (red dashed line) at $\lambda_0 = 1550$ nm. (f and g) Magnetic field profiles for the structure of (a), normal to the plane containing the axes of the coaxial waveguide and coaxial stub resonator. Results are shown for $L = 290$ nm and 460 nm at $\lambda_0 = 1550$ nm, when the fundamental mode of the plasmonic coaxial waveguide is incident from the left.

cavity is far from resonance. Thus, the cavity mode is not excited and the incident waveguide mode is almost completely transmitted [Fig. 2(g)].

Since the distance between the inner and outer metals of the coaxial waveguide is much smaller than the wavelength, only the fundamental quasi-TEM mode of the waveguide [32] propagates. Thus, we can use single-mode scattering matrix theory to account for the behavior of the system [39, 50]. The complex magnetic field reflection coefficients r_1 and r_2, and transmission coefficients t_1, t_2, t_3, and t_4, when the fundamental mode of the plasmonic coaxial waveguide is incident at a T-splitter along two different incident directions are defined as shown in Figs. 2(b) and 2(c). Note that $t_3 = t_4$ due to the mirror symmetry of the structure. In addition, the reflection coefficient r_3 of the fundamental mode of the plasmonic coaxial waveguide at the boundary of a short-circuited coaxial waveguide is defined as shown in Fig. 2(d). The power transmission coefficient of the device can then be calculated using scattering matrix theory as [39, 50]

$$T = |t_1 - C|^2. \tag{1}$$

Here $C = t_2 t_3/(r_2 - s)$, $s = {r_3}^{-1}\exp(2\gamma L)$, and $\gamma = \alpha + i\beta$ is the complex wave vector of the fundamental propagating quasi-TEM mode of the plasmonic coaxial waveguide [39]. The complex magnetic field reflection and transmission coefficients can be numerically extracted using full-wave FDFD simulations [39, 50]. We numerically calculated these coefficients, and the results obtained with scattering matrix theory [Eq. (1)] using this approach (blue solid line) are in excellent agreement with the exact results obtained using FDFD [Fig. 2(e)].

The complex magnetic field reflection and transmission coefficients can also be predicted using transmission line theory and the concept of characteristic impedance [31, 50]. The characteristic impedance of the fundamental quasi-TEM mode of the plasmonic coaxial waveguide is defined as the ratio of electric voltage drop between the inner and outer metals to the electric current flowing through the inner metal

$$Z_0 = \frac{V}{I}. \tag{2}$$

It can be numerically extracted by integrating the E- and H-fields of the mode [20, 32, 51].

Figure 3(a) shows the transmission line model of the plasmonic coaxial waveguide side-coupled to the short-circuited coaxial stub resonator. The model consists of a short-circuited transmission line resonator of length L, propagation constant γ, and characteristic impedance Z_0, which is connected in parallel to a transmission line with the same characteristic impedance Z_0 [32, 37].

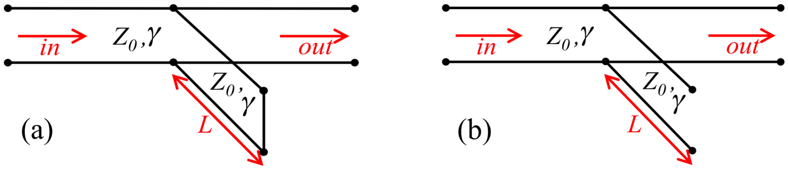

Fig. 3. Schematic of the transmission line model of a plasmonic coaxial waveguide side-coupled to (a) a short-circuited coaxial stub resonator, and (b) an open-circuited coaxial stub resonator. Here Z_0 and γ are the characteristic impedance and complex propagation constant of the fundamental mode of the plasmonic coaxial waveguide.

The complex magnetic field transmission and reflection coefficients in Eq. (1) can then be calculated based on this transmission line model. The T-junction of Fig. 2(b) is equivalent to a junction between three transmission lines in the quasi-static limit. Since all three transmission lines have the same cross sectional shape, they have the same characteristic impedance Z_0 [Fig. 3(a)]. The two output transmission lines are connected in parallel, and the current flowing through the input transmission line is equally divided into the two output lines [32]. The load impedance seen from the input transmission line is therefore $Z_L = Z_0/2$. Thus, the reflection coefficients r_1 and r_2 can be calculated as $r_1 = r_2 = (Z_0/2 - Z_0)/(Z_0/2 + Z_0) = -1/3$ and the transmission coefficients into the output lines are $t_1 = t_2 = t_3 = t_4 = 1 + r_1 = 2/3$. Also $r_3 = (Z_L - Z_0)/(Z_L + Z_0) = -1$, since the stub resonator is short-circuited so that $Z_L = 0$ [Fig. 3(a)] [52].

Figure 2(e) shows the transmission as a function of the stub length L for the structure of Fig. 2(a), predicted by the transmission line model described above (red dashed line). We observe that there is very good agreement between the transmission line model results and the exact results obtained using FDFD, verifying the validity and usefulness of the transmission line model for the plasmonic coaxial waveguide structure of Fig. 2(a). We found that the difference between the transmission line results and the exact numerical results is mostly due to the error introduced by the transmission line model in the phase of the reflection coefficient [37, 53, 54] at the two interfaces of the side-coupled cavity of length L. The predictions of the transmission line model are less accurate compared to the ones of scattering matrix theory with numerically calculated transmission and reflection coefficients [Fig. 2(e)]. However, using the transmission

#242538 Received 8 Jun 2015; revised 16 Jul 2015; accepted 23 Jul 2015; published 28 Jul 2015

line model is a more computationally efficient approach, since it requires only computation of the modes of the waveguide, without the need to simulate the junctions and the waveguide ends.

3. Plasmonic coaxial waveguide side-coupled to an open-circuited coaxial stub resonator

We now consider a waveguide-cavity structure built by side-coupling an open-circuited stub resonator, consisting of a plasmonic coaxial waveguide of finite length, to a plasmonic coaxial waveguide [Fig. 1(c)]. In this case the inner and outer metals at the end of the stub are not connected, and the resonator is therefore open-circuited. Figure 4(a) shows the top view schematic at $z = 0$ of the plasmonic coaxial waveguide, coupled to the open-circuited stub resonator [Fig. 1(e)].

We note that, due to the field profile of the fundamental quasi-TEM mode of the plasmonic coaxial waveguide [32], the power radiated from an open-circuited coaxial waveguide is very small. More specifically, we found that for an open-circuited plasmonic coaxial waveguide with parameters as in Fig. 1(e) operating at $\lambda_0 = 1550$ nm, the power reflection coefficient of the fundamental mode of the waveguide at the boundary is $|r_3|^2 \simeq 0.98$. Thus, the radiation losses for the open-circuited plasmonic coaxial waveguide are very small, and such a waveguide can be used as a resonator in a plasmonic waveguide-cavity device. This is in contrast to open-circuited 2D MDM plasmonic waveguides which cannot be used as resonators, due to the large radiation losses at the waveguide boundary. More specifically, we found that for an open-circuited 2D MDM waveguide with the same materials, metal separation, and operating wavelength as the coaxial waveguide in Fig. 1(e) the power reflection coefficient of the fundamental mode of the waveguide at the boundary is $|r|^2 \simeq 0.68$. Thus, open-circuited 2D MDM waveguides suffer from substantial radiation losses, which are detrimental when such waveguides are used as resonators in plasmonic waveguide-cavity devices.

Figure 4(c) shows the power transmission coefficient of the coaxial waveguide side-coupled to the open-circuited coaxial stub resonator as a function of the stub length L, obtained from full-wave FDFD simulations (dots). We observe that the transmission becomes zero when the length of the stub is approximately equal to 100 nm. As in the case of the short-circuited stub resonator (Section 2), the air-waveguide interface at the boundary of the open-circuited stub, and the inner metal of the main waveguide form a cavity resonator. Since the cavity is short-circuited at one side and open-circuited at the other, its first resonance length will be $L_c = \lambda_g/4 \simeq 170$ nm. The required stub length can therefore be estimated, as in the case of the short-circuited stub resonator (Section 2), as $L = L_c - w \simeq 120$ nm, which is close to the numerically calculated value (100 nm). Similarly, the second resonance length will be $L_c = 3\lambda_g/4 \simeq 510$ nm. Therefore the required stub length for the second resonance can be estimated as $L = L_c - w \simeq 460$ nm, which is the same as the numerically calculated value. We note that for the first resonance the required stub length is $\sim$2.9 times smaller than the required length for a short-circuited stub resonator (Section 2). Thus, using open-circuited plasmonic coaxial stub resonators leads to much more compact waveguide-cavity devices, compared to devices based on short-circuited resonators.

Figures 4(d) and 4(e) show the profile of the H_z field component for two different lengths of the open-circuited stub resonator. For $L = 100$ nm the cavity is on resonance, the directly transmitted wave destructively interferes with the decaying amplitude into the forward direction of the resonant cavity field, and the transmission is therefore approximately zero [Fig. 4(d)]. For $L = 300$ nm the cavity is far from resonance, the cavity mode is not excited, and the incident waveguide mode is therefore almost completely transmitted [Fig. 4(e)].

As in the case of the short-circuited stub resonator (Section 2), we can use single-mode scattering matrix theory to calculate the power transmission coefficient of the device [Eq. (1)]. The reflection coefficient r_3 of the fundamental mode of the plasmonic coaxial waveguide at

#242538 Received 8 Jun 2015; revised 16 Jul 2015; accepted 23 Jul 2015; published 28 Jul 2015

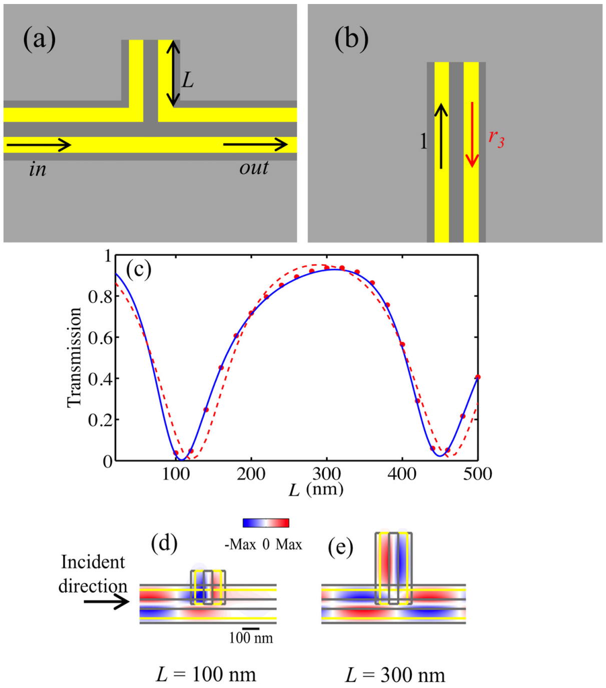

$L = 100$ nm $L = 300$ nm

Fig. 4. (a) Top view schematic at $z = 0$ [Fig. 1(e)] of a plasmonic coaxial waveguide side-coupled to an open-circuited coaxial stub resonator. (b) Schematic defining the reflection coefficient r_3 of the fundamental mode of the plasmonic coaxial waveguide at the boundary of an open-circuited coaxial waveguide. (c) Transmission as a function of the stub length L for the structure of (a) calculated using FDFD (dots), scattering matrix theory with numerically calculated coefficients (blue solid line), and scattering matrix theory with coefficients calculated based on transmission line model (red dashed line) at $\lambda_0 = 1550$ nm. (d and e) Magnetic field profiles for the structure of (a), normal to the plane containing the axes of the coaxial waveguide and coaxial stub resonator. Results are shown for $L = 100$ nm and 300 nm at $\lambda_0 = 1550$ nm, when the fundamental mode of the plasmonic coaxial waveguide is incident from the left.

the boundary of an open-circuited coaxial waveguide is defined as shown in Fig. 4(b). All other transmission and reflection coefficients in Eq. (1) are defined as before [Figs. 2(b) and 2(c)]. We numerically calculated all these coefficients, and the results obtained with scattering matrix theory [Eq. (1)] using this approach (blue solid line) are in excellent agreement with the exact results obtained using FDFD [Fig. 4(c)].

As in the case of the short-circuited stub resonator (Section 2), we can also use transmission line theory to predict the behavior of the system. Figure 3(b) shows the transmission line model of the plasmonic coaxial waveguide side-coupled to the open-circuited coaxial stub resonator, consisting of an open-circuited transmission line resonator connected in parallel to a transmission line with the same characteristic impedance. All complex magnetic field transmission and reflection coefficients in Eq. (1) are calculated based on this transmission line model, similar to the short-circuited stub resonator case. The only difference is that for the open-circuited resonator $Z_L \to \infty$, so that $r_3 = (Z_L - Z_0)/(Z_L + Z_0) = 1$. Similar to the short-circuited stub resonator case, we observe that there is very good agreement between the transmission line model results (red dashed line) and the exact results obtained using FDFD [Fig. 4(c)].

4. Plasmonic coaxial waveguide side-coupled to two open-circuited coaxial stub resonators

We next consider a waveguide-cavity structure built by side-coupling a plasmonic coaxial waveguide to two open-circuited stub resonators, each consisting of a plasmonic coaxial waveguide of finite length [Fig. 1(d)]. We use open-circuited coaxial stub resonators because they lead to much more compact waveguide-cavity devices, compared to short-circuited resonators (Section 3). Figure 5(a) shows the top view schematic at $z = 0$ of the structure [Fig. 1(e)]. This system is a plasmonic classical analogue of EIT [39, 55–58]. Such systems enable enhanced light-matter interaction by slowing down light, and could therefore lead to nanoscale plasmonic devices, such as switches and sensors, with enhanced performance [39].

Figure 5(c) shows the transmission spectra of the coaxial waveguide side-coupled to two open-circuited coaxial stub resonators obtained from full-wave FDFD simulations (dots). The structure exhibits EIT-like transmission spectra, consisting of a transparency peak in the center of a broader transmission dip. The stub lengths L_1 and L_2 are chosen so that the frequency of the transparency peak is $f_0 \simeq 200$ THz.

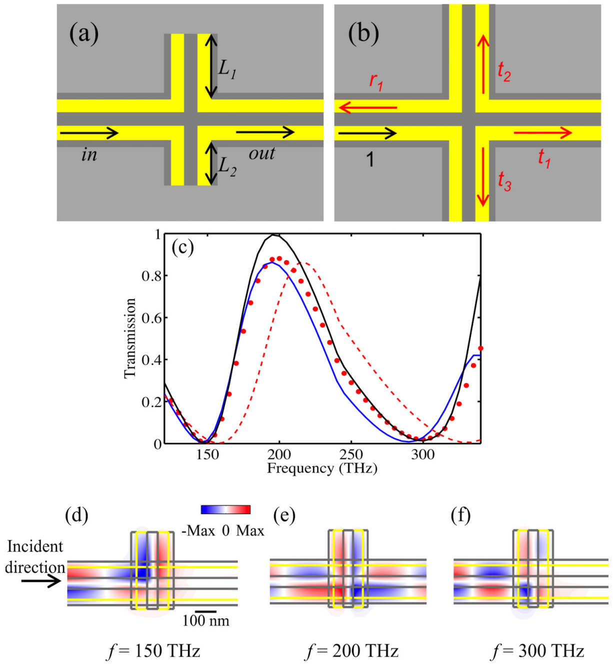

Fig. 5. (a) Top view schematic at $z = 0$ [Fig. 1(e)] of a plasmonic coaxial waveguide side-coupled to two open-circuited coaxial stub resonators. (b) Schematic defining the reflection coefficient r_1, and the transmission coefficients t_1, t_2, and t_3, when the fundamental mode of the plasmonic coaxial waveguide is incident at a waveguide crossing. Note that $t_2 = t_3$ due to symmetry. (c) Transmission spectra for the structure of (a) calculated using FDFD (dots), scattering matrix theory (blue solid line), and transmission line theory (red dashed line). Results are shown for $L_1 = 160$ nm and $L_2 = 42$ nm. Also shown are the transmission spectra calculated using FDFD for lossless metal (black solid line). (d)-(f) Magnetic field profiles for the structure of (a), normal to the plane containing the axes of the coaxial waveguide and coaxial stub resonators. Results are shown for $L_1 = 160$ nm and $L_2 = 42$ nm at $f = 150$, 200, and 300 THz, when the fundamental mode of the plasmonic coaxial waveguide is incident from the left.

#242538 Received 8 Jun 2015; revised 16 Jul 2015; accepted 23 Jul 2015; published 28 Jul 2015

The transmission spectra are very similar to that of a 2D MDM plasmonic waveguide side-coupled to two MDM stub resonators [39]. They feature two dips [Fig. 5(c)] at frequencies f_1 and f_2, which are approximately equal to the resonant frequencies of the two cavities, i.e., $\phi_{r_1}(f_i) + \phi_{r_3}(f_i) - 2\beta(f_i)L_i \simeq -2\pi$, $i = 1,2$, where $\phi_{r_i} = \arg(r_i)$, $i = 1,3$. Here the reflection coefficient r_1 is defined as shown in Fig. 5(b), while r_3 is defined as shown in Fig. 4(b). When either of the cavities is on resonance, the field intensity in that cavity is high, and the transmission is almost zero, since the incoming wave interferes destructively with the decaying amplitude into the forward direction of the resonant cavity field [Figs. 5(d) and 5(f)]. The transmission spectra also feature a transparency peak at frequency f_0, which is approximately equal to the resonant frequency of the composite cavity of length $L_1 + L_2 + w_s$ formed by the two cavities, i.e., $2\phi_{r_3}(f_0) - 2\beta(f_0)(L_1 + L_2 + w_s) \simeq -2\pi$, where $w_s = 150$ nm is the gap between the two stub resonators. When $f = f_0$, the field intensity is high in the entire composite cavity [Fig. 5(e)], and the peak in the spectra is due to resonant tunneling of the incoming wave through the composite cavity. In the lossless metal case, the transparency peak has unity transmission, while in the presence of loss, the peak transmission is lower due to absorption in the resonators [Fig. 5(c)].

As in the case of single resonator structures (Sections 2 and 3), we can use scattering matrix theory to calculate the power transmission coefficient of the device. The reflection coefficient r_1, and transmission coefficients t_1, t_2, and t_3, when the fundamental mode of the plasmonic coaxial waveguide is incident at a waveguide crossing, are defined as shown in Fig. 5(b). Note that $t_2 = t_3$ due to symmetry. The reflection coefficient r_3 at the boundary of an open-circuited coaxial waveguide is defined as before [Fig. 4(b)]. It turns out that the power transmission coefficient of the device can then be calculated again using Eq. (1), where now $C = \frac{{t_2}^2(2t_1 - 2r_1 + s_1 + s_2)}{{t_1}^2 - (r_1 - s_1)(r_1 - s_2)}$, and $s_i = {r_3}^{-1}\exp(2\gamma L_i)$, $i = 1,2$ [39].

The results obtained with scattering matrix theory [Eq. (1)], after numerically calculating the transmission and reflection coefficients (blue solid line), are in very good agreement with the exact results obtained using FDFD [Fig. 5(c)]. The difference between the scattering matrix theory results and the exact numerical results is due to coupling of higher order nonpropagating modes of the waveguides which becomes important because of the deep subwavelength lengths of the resonators [50].

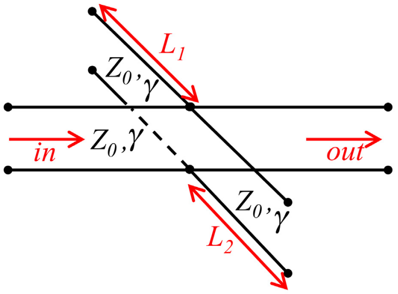

Fig. 6. Schematic of the transmission line model of a plasmonic coaxial waveguide side-coupled to two open-circuited coaxial stub resonators. Here Z_0 and γ are the characteristic impedance and complex propagation constant of the fundamental mode of the plasmonic coaxial waveguide.

Similar to single resonator structures (Sections 2 and 3), we can also use transmission line theory to account for the behavior of the coaxial waveguide side-coupled to two resonators. Figure 6 shows the transmission line model of the structure, consisting of two open-circuited

Received 8 Jun 2015; revised 16 Jul 2015; accepted 23 Jul 2015; published 28 Jul 2015

transmission line resonators connected in parallel to a transmission line with the same characteristic impedance. All transmission and reflection coefficients are calculated based on this model. Thus, the waveguide crossing of Fig. 5(b) is equivalent to a junction between four transmission lines with the same characteristic impedance Z_0. The three output transmission lines are connected in parallel, and the load impedance seen from the input transmission line is therefore $Z_L = Z_0/3$. The reflection coefficient can then be calculated as $r_1 = (Z_0/3 - Z_0)/(Z_0/3 + Z_0) = -1/2$, and the transmission coefficients into the output lines are $t_1 = t_2 = t_3 = 1 + r_1 = 1/2$.

We observe that there is qualitative agreement between the transmission line model results and the exact results obtained using FDFD [Fig. 5(c)]. While the transmission at the transparency peak is correctly predicted by the transmission line model, the peak frequency obtained using transmission line theory is blue-shifted with respect to the FDFD result [Fig. 5(c)]. The reason for the significant difference between the transmission line results and the exact numerical results for the transmission spectra of the coaxial waveguide side-coupled to two resonators is that the spectra result from the interference of two resonant pathways [34]. Despite its limited accuracy for structures with multiple components, the transmission line model is computationally efficient, and, when combined with space mapping algorithms, it could enable the efficient design of nanoplasmonic coaxial waveguide devices [59].

5. Emulation of 2D MDM plasmonic waveguide devices with 3D coaxial waveguide devices

In the previous section, we saw that the transmission spectra of a 3D plasmonic coaxial waveguide side-coupled to two open-circuited coaxial stub resonators are very similar to that of a 2D MDM waveguide side-coupled to two MDM stub resonators. Here we show that, with proper choice of their design parameters, a 3D plasmonic coaxial waveguide-cavity device and a 2D MDM waveguide-cavity device can have nearly identical transmission spectra.

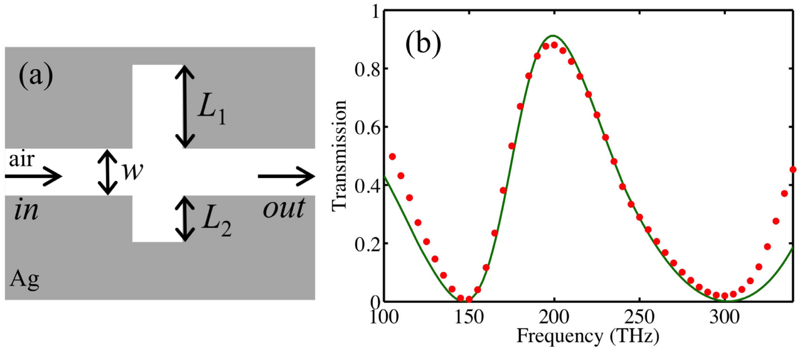

Fig. 7. Emulation of two-dimensional metal-dielectric-metal plasmonic waveguide devices with three-dimensional plasmonic coaxial waveguide devices. (a) Schematic of a two-dimensional silver-air-silver MDM plasmonic waveguide side-coupled to two short-circuited MDM stub resonators. (b) Transmission spectra for the two-dimensional structure of (a) calculated using FDFD for $w = 50$ nm, $L_1 = 354$ nm, and $L_2 = 154$ nm (solid green line). Also shown are the transmission spectra for the three-dimensional structure of Fig. 5(a) calculated using FDFD for $L_1 = 160$ nm and $L_2 = 42$ nm (red dots).

More specifically, we consider a 2D silver-air-silver MDM plasmonic waveguide side-coupled to two short-circuited MDM stub resonators [Fig. 7(a)]. The transmission spectra of the 3D plasmonic coaxial waveguide side-coupled to two open-circuited coaxial stub resonators, which we discussed in the previous section, are shown in Fig. 5(c). We use the space mapping algorithm [59] to find the optimum match between the responses of the 2D [Fig. 7(a)] and 3D [Fig. 1(d)] plasmonic waveguide devices. Using this approach, we find that, when the stub lengths L_1 and L_2 of the 2D MDM device [Fig. 7(a)] are optimized, its transmission spectra almost exactly match the spectra of the 3D device [Fig. 7(b)].

While here we found a 2D structure which matches the response of a 3D structure, the opposite process is also possible: we can use the space mapping algorithm [59] to find a 3D structure with nearly identical response to that of a 2D structure. This is particularly useful for the practical implementation of plasmonic waveguide-cavity devices. Most of the theoretical investigations of plasmonic waveguide-cavity systems have focused on 2D structures [33–44]. This is due to the smaller computational cost of full-wave electromagnetic simulations in 2D compared to 3D, as well as the simplicity of visualizing and understanding the underlying optical physics in 2D [60]. However, practical realization of these waveguide-cavity systems requires the use of 3D structures. Since with proper choice of design parameters 3D plasmonic coaxial waveguide-cavity devices can have nearly identical transmission spectra to that of 2D MDM devices, the 2D designs can be translated into 3D designs suitable for experimental realization. Thus, 3D plasmonic coaxial waveguides offer a platform for practical implementation of 2D MDM devices.

6. Conclusions

In this paper, we theoretically investigated 3D plasmonic waveguide-cavity structures, built by side-coupling stub resonators that consist of plasmonic coaxial waveguides of finite length, to a plasmonic coaxial waveguide. We used plasmonic coaxial waveguides with square cross section which can be fabricated using lithography-based techniques.

We first investigated structures consisting of a single plasmonic coaxial resonator, which is terminated in a short circuit. The power transmission characteristics of the device were investigated using the 3D FDFD method. We showed that the incident waveguide mode is almost completely reflected on resonance, while far from the resonance the waveguide mode is almost completely transmitted. We also showed that the properties of this waveguide-cavity system can be accurately described using a single-mode scattering matrix theory. The transmission and reflection coefficients at waveguide junctions can be numerically extracted using full-wave simulations, and the results obtained with scattering matrix theory using this approach are in excellent agreement with the exact results. These coefficients can also be predicted using transmission line theory and the concept of characteristic impedance. We found that there is very good agreement between the transmission line model results and the exact results obtained using FDFD, verifying the validity and usefulness of the transmission line model for this plasmonic coaxial waveguide structure.

We next investigated structures consisting of a single plasmonic coaxial resonator, which is terminated in an open circuit. We found that, in contrast to open-circuited 2D MDM plasmonic waveguides which suffer from large radiation losses, open-circuited plasmonic coaxial waveguides have very small radiation losses, and can therefore be used as resonators in waveguide-cavity devices. We also found that using open-circuited plasmonic coaxial stub resonators leads to much more compact waveguide-cavity devices, compared to devices based on short-circuited resonators.

We next considered waveguide-cavity structures built by side-coupling a plasmonic coaxial waveguide to two open-circuited stub resonators. We showed that this structure is a plasmonic classical analogue of EIT, and its transmission spectra consist of a transparency peak in the center of a broader transmission dip. We found that these spectra are very similar to that of a 2D MDM plasmonic waveguide side-coupled to two MDM stub resonators. We also found that for this structure there are differences between the scattering matrix theory results and the exact

#242538 Received 8 Jun 2015; revised 16 Jul 2015; accepted 23 Jul 2015; published 28 Jul 2015

numerical results, due to coupling of higher order nonpropagating modes of the waveguides. In addition, the peak frequency obtained using transmission line theory is blue-shifted with respect to the exact result, because in this case the spectra result from the interference of two resonant pathways. Despite its limited accuracy for structures with multiple components, the transmission line model is computationally efficient, and, when combined with space mapping algorithms, it could enable the efficient design of nanoplasmonic coaxial waveguide devices.

Finally we showed that, with proper choice of their design parameters, 3D plasmonic coaxial waveguide-cavity devices and 2D MDM devices can have nearly identical transmission spectra. More specifically, we used the space mapping algorithm to find the optimum match between the responses of a 2D and a 3D device, and found that, using this approach, the transmission spectra of the 2D device almost exactly match the spectra of the 3D device. Thus, 3D plasmonic coaxial waveguides offer a platform for practical implementation of 2D MDM device designs.

As final remarks, we note that in plasmonic coaxial waveguides the propagation length of the fundamental propagating mode is limited by material loss in the metal. As an example, the propagation length of the fundamental mode of the plasmonic coaxial waveguide of Fig. 1(e) for $\lambda_0 = 1550$ nm is $L_p = 6.82\ \mu$m [32]. Thus, for longer distances dielectric waveguides will have to be used to carry the optical signal [61]. Couplers between plasmonic coaxial waveguides and dielectric waveguides will therefore be essential components for integrated photonics applications.

Acknowledgments

This research was supported by the Louisiana Board of Regents (contract LEQSF-EPS(2014)-PFUND-358), the National Science Foundation (Awards No. 1102301 and 1254934), and the U. S. Air Force Office of Scientific Research (FA9550-12-1-0024).